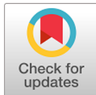

Research Article | Vol. 27, No. 19 | 16 Sep 2019 | OPTICS EXPRESS 26882

Optics EXPRESS

Enhancing Pockels effect in strained silicon waveguides

IRENE OLIVARES, JORGE PARRA, ANTOINE BRIMONT, AND PABLO SANCHIS*

Nanophotonics Technology Center, Universitat Politècnica de València, Camino de Vera s/n, 46022 Valencia, Spain

*pabsanki@ntc.upv.es

Abstract: The magnitude and origin of the electro-optic measurements in strained silicon devices has been lately the object of a great controversy. Furthermore, recent works underline the importance of the masking effect of free carriers in strained waveguides and the low interaction between the mode and the highly strained areas. In the present work, the use of a p-i-n junction and an asymmetric cladding is proposed to eliminate the unwanted carrier influence and improve the electro-optical modulation response. The proposed configuration enhances the effective refractive index due to the strain-induced Pockels effect in more than two orders of magnitude with respect to the usual configuration.

© 2019 Optical Society of America under the terms of the OSA Open Access Publishing Agreement

1. Introduction

The silicon platform offers an enormous potential for integrated photonics due to the possibility of combining photonic and electronics on the same chip. Moreover, photonics can benefit from the mature fabrication processes, capabilities and know-how of the microelectronic industry, enabling a low cost and high-volume CMOS compatible production of photonic integrated circuits (PICs). However, although the variety of functionalities is continuously expanding, one of the main limiting factors is the material itself. The lack of electro-optical activity in silicon due to its crystal centrosymmetry prevents the development of key components in this platform. Applications such as nonlinear phenomena or high-speed efficient modulation are currently addressed either by integrating III-V compounds [1], ferroelectric materials, such as $LiNbO_3$ [2] or $BaTiO_3$ [3], and organic compounds [4] or by relying in the plasma dispersion effect for optical modulation [5]. In this context, strained silicon was proposed more than ten years ago as a disruptive approach to tackle this problem [6]. Due to the broken symmetry induced by the applied strain, the second order susceptibility is no longer inhibited and high speed and low power electro-optical modulation is allowed based on the Pockels effect [7]. Some phenomenological models have been reported [8,9] and, by studying stress, the lattice symmetry and waveguide geometry [10–12] electro-optical modulation has been shown and optimized on this technology and used to extract large second-order susceptibility values [12–14]. However, the origin of the measured data has been questioned in recent studies and the important role played by free and trapped carriers in masking the underlying Pockels effect has been emphasized [15–20]. It has also been suggested that the observed nonlinearities could arise not from the strained silicon but from the silicon nitride layer covering the structures [21]. Furthermore, theoretical models [22,23] and second-harmonic generation experiments predict much lower values for the second order susceptibility [24–27]. Recently, high frequency modulation has been demonstrated in a strained Mach-Zehnder interferometer but with an effective susceptibility value of a few pm/V [28]. On the other hand, almost a year ago, strong high frequency modulation was demonstrated via third-order susceptibility in a silicon waveguide. A p-i-n junction was used to extract the free carriers from the waveguide core and enhance the weak Kerr effect present in silicon [29]. In this letter the use of a similar p-i-n structure in a strained silicon waveguide

#367870 https://doi.org/10.1364/OE.27.026882
Journal © 2019 Received 20 May 2019; revised 5 Jul 2019; accepted 8 Jul 2019; published 11 Sep 2019

is proposed to overcome the masking effect of carriers and, thus, enhance the strain induced Pockels effect. In addition, an asymmetric cladding is also used to improve the overlap between the strain and the optical modes. As a result, effective index change values of more than two orders of magnitude higher than those obtained for the undoped structure have been predicted.

2. The index ellipsoid in strained silicon

Figure 1(a) shows the initial considered structure, consisting on a silicon rib waveguide of 400 × 220 nm^2 with an etching depth of 140 nm and a background acceptor doping of 10^{15} cm^{-3} covered by a silicon nitride layer that acts as a stressor. The cladding thickness has been chosen to be 700 nm with a compressive intrinsic stress of 2 GPa. As depicted in Fig. 1(b), the waveguide is rotated around its vertical axis to study the effect of the crystal orientation on the second order susceptibility tensor. The rotation angle, ϕ, is defined with respect to the initial coordinate system, which is aligned with the principal axes of a cubic crystal, i.e. x' = [100], y' = [001], z' = [0-10]. Thus, the four bond vectors of the primitive cell, shown in the inset of Fig. 1(b), must be written as a function of ϕ:

$$\begin{aligned}
\xi_1 &= \frac{d}{\sqrt{3}}\left(\cos\phi+\sin\phi, 1, \sin\phi-\cos\phi\right) \\
\xi_2 &= \frac{d}{\sqrt{3}}\left(\cos\phi-\sin\phi, -1, \sin\phi+\cos\phi\right) \\
\xi_3 &= \frac{d}{\sqrt{3}}\left(-\cos\phi+\sin\phi, -1, -\sin\phi-\cos\phi\right) \\
\xi_4 &= \frac{d}{\sqrt{3}}\left(-\cos\phi-\sin\phi, 1, -\sin\phi+\cos\phi\right)
\end{aligned} \tag{1}$$

being d = 0.235 nm the length of the unstrained Si-Si bonds. In addition, the silicon has been considered as an anisotropic material and the variation of the strain with the rotation of the waveguide has also been taken into account [30,31].

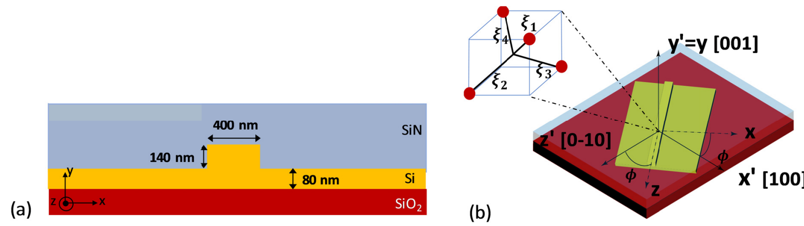

Fig. 1. (a) Sketch of the strained silicon waveguide covered with a silicon nitride layer of 700 nm and a compressive stress of 2 GPa, and (b) representation of the rotated waveguide showing the reference and waveguide coordinate systems. The reference system is aligned with the crystalline directions of a cubic crystal x' = [100], y' = [001], z' = [0-10]. The four bond vectors of the silicon primitive cell are displayed in the inset.

Using Eq. (1) and the bond orbital model described in [22], it is possible to obtain the second order susceptibility tensor as a function of ϕ and the strain gradients inside the waveguide core:

$$\chi^{(2)} = \begin{bmatrix} \chi^{(2)}_{11}(\phi) & \chi^{(2)}_{12}(\phi) & \chi^{(2)}_{13}(\phi) & \chi^{(2)}_{14}(\phi) & \chi^{(2)}_{15}(\phi) & \chi^{(2)}_{16}(\phi) \\ \chi^{(2)}_{21}(\phi) & \chi^{(2)}_{22}(\phi) & \chi^{(2)}_{23}(\phi) & 0 & \chi^{(2)}_{25}(\phi) & \chi^{(2)}_{26}(\phi) \\ \chi^{(2)}_{31}(\phi) & \chi^{(2)}_{32}(\phi) & \chi^{(2)}_{33}(\phi) & \chi^{(2)}_{34}(\phi) & \chi^{(2)}_{35}(\phi) & \chi^{(2)}_{36}(\phi) \end{bmatrix}, \tag{2}$$

Optics EXPRESS

where contracted notation has been used for j (1→11, 2→22, 3→33, 4→23, 5→13, 6→12). The explicit expressions for the susceptibility coefficients have been omitted for clarity and can be found in the Appendix A along with a more exhaustive analysis of their dependency on ϕ. It is important to highlight, however, that all of them are in the same order of magnitude and vary between negligible values at the waveguide center up to several pm/V near the waveguide walls, where the strain is higher. Once we know the susceptibility tensor, the index ellipsoid can be calculated by using its general formula [32]:

$$\left(\eta_{ij} + \Delta\eta_{ij}\right) x_i x_j = 1 \tag{3}$$

being x_i = x, y or z for i = 1,2 or 3, respectively, and analogously for x_j, $\eta_{ij} = \varepsilon_o^{-1}$ the impermeability tensor of unstrained silicon and $\Delta\eta_{ij}$ the perturbation induced by the Pockels effect, which is given by

$$\begin{bmatrix} \Delta\eta_{xx} \\ \Delta\eta_{yy} \\ \Delta\eta_{zz} \\ \Delta\eta_{yz} \\ \Delta\eta_{xz} \\ \Delta\eta_{xy} \end{bmatrix} = \begin{bmatrix} r_{11} & r_{12} & r_{13} \\ r_{21} & r_{22} & r_{23} \\ r_{31} & r_{32} & r_{33} \\ r_{41} & 0 & r_{43} \\ r_{51} & r_{52} & r_{53} \\ r_{61} & r_{62} & r_{63} \end{bmatrix} \cdot \begin{bmatrix} E_x \\ E_y \\ E_z \end{bmatrix}. \tag{4}$$

The applied electric field along the propagation direction E_z has been assumed to be zero and the Pockels coefficients r_{ij} have been obtained from the susceptibility tensor by using the relationship $r_{ij} = -\frac{2}{n_o^4}\chi_{ij}^{(2)}$ [32], with n_0 = 3.454 the index of unstrained silicon. The resultant index ellipsoid has, in general, non-negligible values for all terms:

$$\begin{aligned} &\left(\frac{1}{n_o^2} + r_{11}E_x + r_{12}E_y\right)x^2 + \left(\frac{1}{n_o^2} + r_{21}E_x + r_{22}E_y\right)y^2 + \left(\frac{1}{n_o^2} + r_{31}E_x + r_{32}E_y\right)z^2 + \\ &2r_{41}E_x yz + 2\left(r_{51}E_x + r_{52}E_y\right)xz + 2\left(r_{61}E_x + r_{62}E_y\right)xy = 1. \end{aligned} \tag{5}$$

Although we cannot diagonalize the index ellipsoid without disregarding any term, it is possible to extract the explicit form of the refractive index matrix by knowing that [32]

$$\left(\eta_{ij} + \Delta\eta_{ij}\right) = \varepsilon^{-1} = \left(n \cdot n\right)^{-1}, \tag{6}$$

where n is the refractive index matrix in the waveguide coordinate system. Furthermore, we can define the index change due to Pockels effect for a given applied voltage as $\Delta n_{ij}^V = \Delta n_{ij}\left(V \neq 0\right) - \Delta n_{ij}\left(V = 0\right)$:

Optics EXPRESS

$$\begin{aligned}
\Delta n_{xx}^{V} &\approx -\frac{1}{2} n_o^3 \left(r_{11} E_x + r_{12} E_y \right) \\
\Delta n_{yy}^{V} &\approx -\frac{1}{2} n_o^3 \left(r_{21} E_x + r_{22} E_y \right) \\
\Delta n_{zz}^{V} &\approx -\frac{1}{2} n_o^3 \left(r_{31} E_x + r_{32} E_y \right) \\
\Delta n_{yz}^{V} &\approx -\frac{1}{2} n_o^3 r_{41} E_x \\
\Delta n_{xz}^{V} &\approx -\frac{1}{2} n_o^2 \left(r_{51} E_x + r_{52} E_y \right) \\
\Delta n_{xy}^{V} &\approx -\frac{1}{2} n_o^2 \left(r_{61} E_x + r_{62} E_y \right).
\end{aligned} \tag{7}$$

As it is possible to see from Eq. (7), the effective index change is directly proportional to the Pockels coefficients and the applied electric field, therefore, it should be possible to find an optimum waveguide orientation and electrode configuration that maximize the index change.

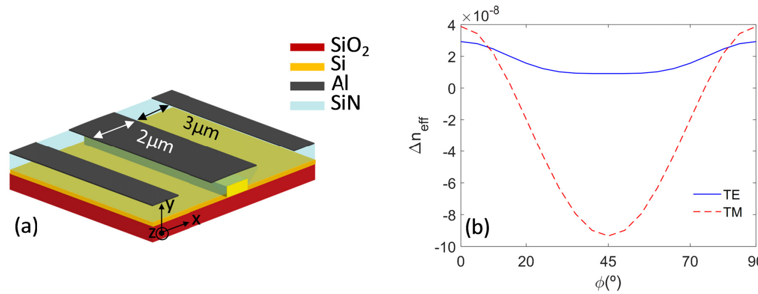

Fig. 2. (a) Sketch of the electrode configuration used to study the strain induced electro-optic effect and the corresponding effective index change for (b) TE (blue) and TM (red) modes as a function of ϕ for an applied voltage of −15 V.

We will start first by studying the electrode configuration used in most experimental works on strained silicon [8–10,14–17,22], which is depicted in Fig. 2(a). The voltage is applied in the central electrode while the laterals are electrically grounded. The space and width of the electrodes have been optimized to 3 µm and 2 µm, respectively, to reach maximum effective index variation. By using Eq. (7), the effective index change as a function of ϕ has been obtained at the working wavelength (λ = 1.55 µm) by using a FEM (finite element method) based software (COMSOL). The result is depicted in Fig. 2(b) for TE and TM modes and an applied voltage of −15 V. All refractive index elements have been considered in this calculation, however, crossed terms play in general a secondary role in the determination of the mode effective index change, as it is more extensively shown in the Appendix B. A remarkable variation with ϕ is predicted specially for the TM mode, varying between negative and positive values. In fact, a null effective index change is predicted for 25° and 65° and reaches a highest negative value of -9×10^{-8} at 45°. This variation with ϕ is related not only to the change in the refractive index but also due to the variation of its distribution inside the waveguide core and, therefore, in the overlap with the optical mode. To show this more clearly, the index change of the Δn_{yy}^{V} element (which is specially influent in the TM mode) is depicted in Fig. 3(a) at ϕ = 0° (top) and ϕ = 45° (bottom) for an applied voltage of −15 V. A quite strong change from positive to negative values can be observed near the waveguide walls between both situations, change that is then reflected in the variation of the effective index when the waveguide is rotated.

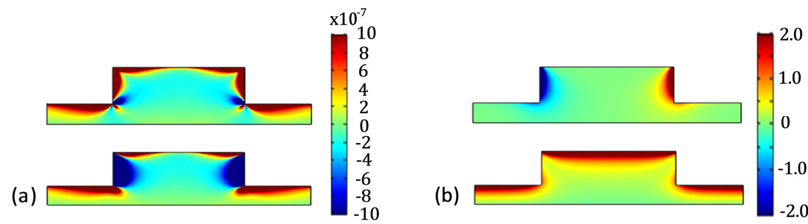

Fig. 3. (a) Contour plot of Δn_{yy}^{V} at ϕ = 0° (top) and ϕ = 45° (bottom) for an applied voltage of −15V and (b) contour plot of the E_x (top) and E_y (bottom) DC electric field components (V/µm).

On the other hand, both TE and TM modes reach the highest positive values of 3×10^{-8} and 4×10^{-8}, respectively, at 0°, which is still very low in comparison with that obtained by the plasma dispersion effect. The explanation of these low results can be attributed to different origins. First, there is an intrinsic limitation due to the small Pockels coefficients we are considering, which are derived using the theoretical model reported in [22] and described more exhaustively in Appendix A. The values of the modelling parameters have been taken from [28], where experimental results were used to extract such values. In addition, there is an attenuation of the Δn_{yy}^{V} due to the location of both, the electric field and the strain gradients at the waveguide borders, areas with little interaction with the optical mode. The first effect is well captured in Fig. 3(b), where the electric field inside the waveguide core is depicted. The electric field is quite strong at the waveguide borders. However, it is screened due to the carrier accumulation at the Si-SiN interface and rapidly decreases to almost negligible values at the waveguide center. We can observe the same trend in Fig. 3(a), where the change in the refractive index elements is strong near the Si-SiN interfaces but decreases several orders of magnitude when approaching the waveguide core. Finally, the effective index change due to plasma dispersion effect has also been simulated, obtaining values around 7.4×10^{-5} for an applied voltage of −15V, i.e. three orders of magnitude higher than those predicted for the strain induced Pockels effect and, thus, completely masking it in static measurements.

3. The effect of a p-i-n junction

As it has been briefly discussed before, the screening of the electric field is one of the main factors limiting the strength of Pockels effect. In this second section, the use of a p-i-n junction is going to be studied to overcome this problem. To do so, highly doped regions are placed at both sides of the waveguide core with an opposite dopant concentration of 10^{20} cm^{-3}. The distance from the waveguide center is chosen to be 400 nm to avoid high absorption losses due to the interaction between the optical field and the highly doped areas. We will begin by studying the behavior of the p-i-n junction with the same electrode configuration as that used in the undoped case, depicted in the top image of Fig. 4(a). In this case, for low values of the applied reverse bias, the junction keeps the free carriers outside the waveguide core and avoids their masking effect. However, for higher applied voltages, the external electric field becomes stronger than the built-in electric field of the junction. In this situation, the external field easily moves the carriers from the highly doped regions to the waveguide core, therefore, cancelling the beneficial effect of the p-i-n structure. In order to avoid this scenario, lateral electrodes have been designed to be in contact with the p^{++} and n^{++} areas, as depicted in the top image of Fig. 4(b). Therefore, the external voltage will be applied not only on the central but also on the lateral electrode contacting the p^{++} region. In this way, the horizontal field created by the p-i-n junction will be strengthened with the applied voltage and will keep the free carriers away from the core. On the other hand, the central electrode will be mainly in charge of enhancing the vertical electric field.

Optics EXPRESS

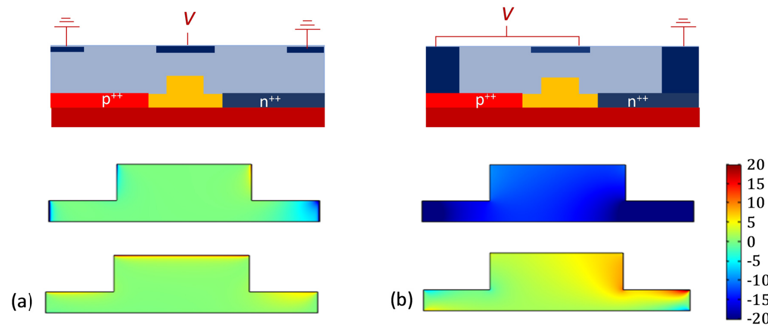

Fig. 4. (a) Sketch of the configuration 1 (top) and contour plot of the E_x (middle) and E_y (bottom) components of the electric field inside the waveguide core (V/μm). (b) Sketch of the configuration 2 (top) and contour plot of the E_x (middle) and E_y (bottom) electric fields inside the waveguide core for this configuration.

Figures 4(a) and 4(b) show the E_x (middle images) and E_y (bottom images) components of the electric field inside the waveguide core for the p-i-n junction with top and top plus lateral electrodes, respectively, which will be referred to in the following as "configuration 1" and "configuration 2". A strong improvement is clearly observed for the latter configuration, in which both E_x and E_y components of the electric field reach values of several and even tens Volts per micron at the waveguide center, while in the first situation the field does not reach 1 V/μm.

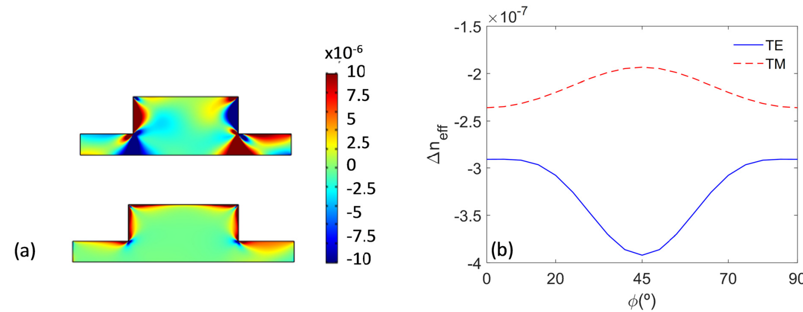

Fig. 5. (a) Contour plot of Δn_{yy}^{V} for the configuration 1 (bottom) and configuration 2 (top) at ϕ = 0° for an applied voltage of −15 V and (b) corresponding effective index change for TE and TM modes.

Thanks to the electric field enhancement, the refractive index change values are improved by around two orders of magnitude with respect to those obtained with the standard configuration. This can be observed in Fig. 5(a), which shows the index change of the Δn_{yy}^{V} element for the configuration 1 (bottom) and configuration 2 (top) at ϕ = 0° for an applied voltage of −15 V. However, the resulting effective index change is a complex combination of the overlap between optical fields and Δn_{yy}^{V}, which results in a lower effective index change. As observed in Fig. 5(b), the best results are obtained at ϕ = 0° for TM and at 45° for TE with values of -2.3×10^{-7} and -3.9×10^{-7}, respectively. This implies an improvement of a factor of 7.6 and 4.3 for TE and TM modes with respect to the best cases of the initial structure. At the same time, the effective index change due to plasma dispersion effect decreases to around 10^{-5}, which is 7.4 times smaller with respect to the initial case.

Optics EXPRESS

4. The effect of an asymmetric cladding

Although high values around 10^{-5} are observed in some areas of Fig. 5(a) for the configuration 2, the low interaction with the optical mode and the overlapping with areas of opposite Δn_{yy}^{V} gives a resulting effective index change of around 10^{-7}, i.e. two orders of magnitude weaker. In order to improve this situation, the use of an asymmetric cladding is analyzed in this section. A scheme of the structure is depicted in Fig. 6(a). Half of the waveguide is covered by a silicon nitride cladding with a high compressive stress of 2 GPa while the other half is covered by a silicon nitride with a tensile stress of 1.25 GPa. Both chosen values are feasible and already experimentally demonstrated in different published works [19,26]. Figure 6(b) shows the contour plot of the Δn_{yy}^{V} element of the refractive index matrix. Thanks to the asymmetry in the applied deformation, a high strain is located at the waveguide center. In addition, most of the waveguide core has an index change of the same sign, which results in a remarkable improvement of the overlap with the optical mode.

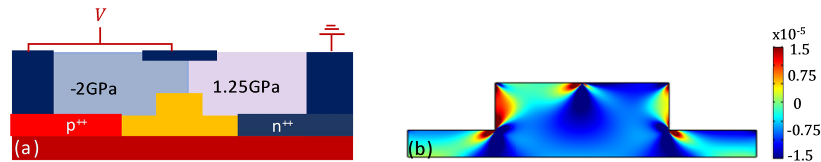

Fig. 6. (a) Sketch of the proposed structure with the left half of the cladding with a compressive stress of 2 GPa (light blue) and the right half with a tensile stress of 1.25 GPa (violet) and (b) contour plot of the Δn_{yy}^{V} refractive index element for $\phi = 0°$ and an applied voltage of −15 V.

In this case, the maximum effective index change increased up to -6×10^{-6} for TE at a rotation angle of $\phi = 0°$, as shown in Fig. 7. Such result represents an increase of more than two orders of magnitude with respect to the initial configuration. Furthermore, a noticeable result is also obtained for the TM mode, with a maximum effective index change of $-3 \cdot 10^{-6}$ also for $\phi = 0°$.

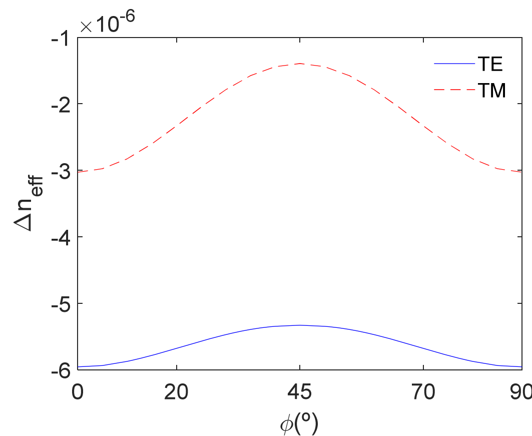

Fig. 7. Effective index change for TE and TM modes as a function of ϕ for an applied voltage of −15 V.

5. Conclusions

The ability of enabling a practical Pockels effect in the silicon platform is currently the subject of a high interest. Strained silicon is clearly the simplest way to achieve that goal.

However, there are two main limiting factors hindering the effect of strain induced Pockels coefficients: the localization of strain and electric field outside the waveguide core. In this work, two methods are proposed to improve each of these problems. First, the use of a p-i-n junction with top and lateral electrodes is proposed to keep the carriers away from the waveguide core and enhance, at the same time, the vertical and horizontal electric fields. Secondly, an asymmetric cladding is used to induce strain in the waveguide core center, which strongly improves the overlap with the optical mode. the proposed methods offer a significant improvement of the effective index change by a factor of 200 with respect to the conventional structure considered until now. It is also important to highlight that such improvement is independent of the modelling parameters used to calculate the Pockels coefficients. The obtained results represent a significant advance in the performance of strained silicon devices and, in addition, it could help to unambiguously demonstrate Pockels effect as the cause of the measured electro-optic response.

Appendix A: explicit form of the second order susceptibility tensor

As explained in the main text, the second order susceptibility tensor is obtained as a function of the waveguide rotation angle, however, the explicit expressions have not been given there for clarity. These expressions have been obtained using the bond orbital model described in [22]. Concretely, the tensor coefficients that have been used to obtain the results presented in this work are the following:

$$\chi_{11}^{(2)} = \frac{Kd^6}{2\cdot 27\varepsilon_o}\left\{\begin{aligned}&\left(7\beta-5\alpha+(3\alpha-\beta)\cos(4\phi)\right)\cdot\eta_{111}+\\&\left(9\beta-3\alpha+(\alpha-3\beta)\cos(4\phi)\right)\cdot\eta_{221}+\\&\left(11\beta-\alpha-(\alpha+5\beta)\cos(4\phi)\right)\cdot\eta_{331}\end{aligned}\right\} \tag{8}$$

$$\chi_{12}^{(2)} = \frac{Kd^6}{2\cdot 27\varepsilon_o}\left\{\begin{aligned}&\left(5\beta-3\alpha+(\alpha+\beta)\cos(4\phi)\right)\cdot\eta_{111}+\\&2(3\alpha-\beta)\cdot\eta_{221}+\left(7\beta-\alpha-(\alpha+\beta)\cos(4\phi)\right)\cdot\eta_{331}\end{aligned}\right\} \tag{9}$$

$$\chi_{13}^{(2)} = \frac{Kd^6}{2\cdot 27\varepsilon_o}\left\{(3\beta-\alpha)\left(\cos(4\phi)+1\right)\left(\eta_{111}+\eta_{221}+\eta_{331}\right)\right\} \tag{10}$$

$$\chi_{14}^{(2)} = \frac{Kd^6}{27\varepsilon_o}\sin(4\phi)(\alpha+\beta)\left(\eta_{112}-\eta_{332}\right) \tag{11}$$

$$\chi_{15}^{(2)} = \frac{2Kd^6}{27\varepsilon_o}\cos(2\phi)\left\{\begin{aligned}&\left(2\beta-2\alpha+(\alpha+\beta)\cos(2\phi)^2\right)\cdot\eta_{111}+\\&(3\beta-\alpha)\cdot\eta_{221}+\left(4\beta-(\alpha+\beta)\cos(2\phi)^2\right)\cdot\eta_{331}\end{aligned}\right\} \tag{12}$$

$$\chi_{16}^{(2)} = \frac{Kd^6}{27\varepsilon_o}\left\{\begin{aligned}&\left(5\beta-3\alpha+(\alpha+\beta)\cos(4\phi)\right)\cdot\eta_{112}+\\&2(3\beta-\alpha)\cdot\eta_{222}+\left(7\beta-\alpha-(\alpha+\beta)\cos(4\phi)\right)\cdot\eta_{332}\end{aligned}\right\} \tag{13}$$

$$\chi_{21}^{(2)} = \frac{Kd^6}{2\cdot 27\varepsilon_o}\left\{\begin{aligned}&\left(5\beta-3\alpha+(\alpha+\beta)\cos(4\phi)\right)\cdot\eta_{112}+\\&2(3\beta-\alpha)\cdot\eta_{222}+\left(7\beta-\alpha-(\alpha+\beta)\cos(4\phi)\right)\cdot\eta_{332}\end{aligned}\right\} \tag{14}$$

$$\chi_{22}^{(2)} = \frac{Kd^6}{27\varepsilon_o}\left\{(3\beta-\alpha)\left(\eta_{112}+\eta_{222}+\eta_{332}\right)\right\} \tag{15}$$

$$\chi_{23}^{(2)}=\frac{Kd^6}{2\cdot 27\varepsilon_o}\left\{\begin{aligned}&(7\beta-\alpha-(\alpha+\beta)\cos(4\phi))\cdot\eta_{112}+\\&2(3\beta-\alpha)\cdot\eta_{222}+(5\beta+(\alpha+\beta)\cos(4\phi))\cdot\eta_{332}\end{aligned}\right\} \tag{16}$$

$$\chi_{24}^{(2)}=0 \tag{17}$$

$$\chi_{25}^{(2)}=\frac{2Kd^6}{27\varepsilon_o}\cos(2\phi)(3\beta-\alpha)(\eta_{112}+\eta_{222}+\eta_{332}) \tag{18}$$

$$\chi_{26}^{(2)}=\frac{Kd^6}{27\varepsilon_o}\left\{\begin{aligned}&(5\beta-3\alpha+(\alpha+\beta)\cos(4\phi))\cdot\eta_{111}+\\&2(3\beta-\alpha)\cdot\eta_{221}+(7\beta-\alpha-(\alpha+\beta)\cos(4\phi))\cdot\eta_{331}\end{aligned}\right\}, \tag{19}$$

where $\eta_{111}=\frac{\partial\varepsilon_{xx}}{\partial x},\eta_{221}=\frac{\partial\varepsilon_{yy}}{\partial x},\eta_{112}=\frac{\partial\varepsilon_{xx}}{\partial y},\eta_{222}=\frac{\partial\varepsilon_{yy}}{\partial y}$, K = -1.18×10^{29} C^3/cm^3eV^3, d = 0.235 nm the length of the unstrained Si-Si bonds and ε_o = 8.85 × 10^{-12} $F\cdot m^{-1}$ the vacuum permittivity. The modelling parameters $\alpha=-5.1\cdot 10^{-16}\frac{\varepsilon_o}{Kd^6}$ and $\beta=-24.6\cdot 10^{-16}\frac{\varepsilon_o}{Kd^6}$ have been taken from [28], where experimental results were used to extract such values. The effect of both types of gradients are completely decouple, that is, the coefficients are either dependent on the horizontal $\left(\chi_{11}^{(2)},\chi_{12}^{(2)},\chi_{13}^{(2)},\chi_{15}^{(2)},\chi_{26}^{(2)}\right)$ or on the vertical strain gradients $\left(\chi_{21}^{(2)},\chi_{22}^{(2)},\chi_{23}^{(2)},\chi_{25}^{(2)},\chi_{16}^{(2)},\chi_{14}^{(2)}\right)$ but never dependent on both.

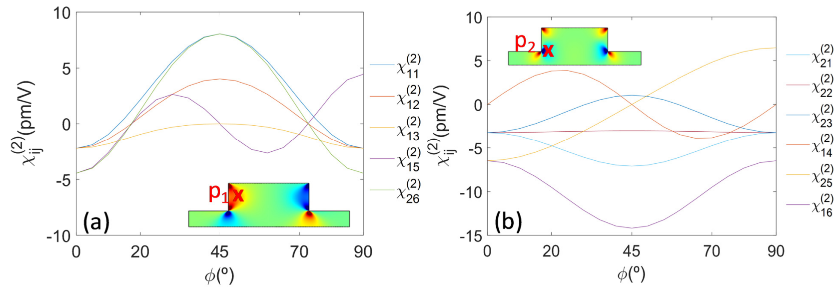

Fig. 8. Rotational dependency of the susceptibility coefficients dependent on (a) the horizontal and (b) vertical strain gradients taken at p_1 and p_2, respectively. The insets show the η_{111} and η_{112} strain gradients as well as the chosen points p_1 and p_2, respectively.

To have an idea about the magnitude of the obtained coefficients and how they vary with the rotation of the waveguide, they have been represented in Figs. 8(a) and 8(b). The coefficients shown in Fig. 8(a) depend only in η_{ij1}. Their values have been taken at a point where η_{ij1} are maximum. The chosen point, p_1(–0.16,0.14) µm, and the η_{111} strain gradient are shown in the inset of Fig. 8(a). Analogously, the coefficients shown in Fig. 8(b) depend only on η_{ij2} and their values have been taken at point p_2 (–0.16,0.07) µm, where the vertical strain gradients are highest. This can be confirmed in the inset of Fig. 8(b), where η_{112} and p_2 are depicted.

Appendix B: contribution of the refractive index crossed terms

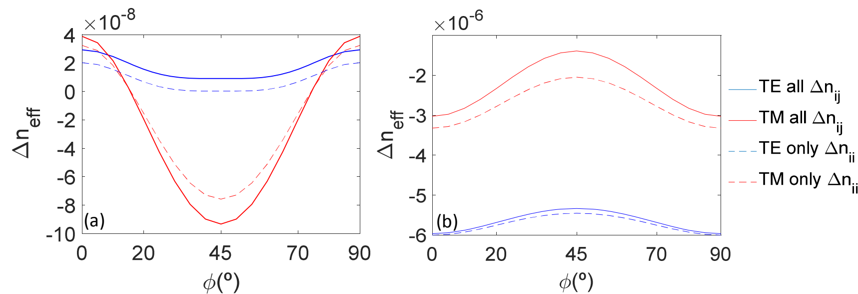

Fig. 9. Effective index change for TE and TM modes for (a) the initial and (b) the optimized structures with an applied voltage of −15V. The depicted results are obtained either by considering all refractive index elements (solid lines) or only diagonal elements (dashed lines).

Figure 9 shows the effective index change for TE and TM modes for Fig. 9(a) the initial and 9(b) optimized structure. In addition to the total effective index change (solid lines) already shown in the main text, the Δn_{eff} obtained by only considering the diagonal Δn_{ii}^{V} terms has also been included (dashed lines). The plotted data shows the weaker contribution of the crossed terms played in the obtained results.

Funding

Ministerio de Economía y Competitividad (MINECO/FEDER, UE) (TEC2016-76849); Universitat Politècnica de València (FPI-Irene Olivares); Ministerio de Educación, Cultura y Deporte (FPU17/04224); Generalitat Valenciana.

Acknowledgments

Irene Olivares and Jorge Parra acknowledges the Universitat Politècnica de València and Generalitat Valenciana, respectively, for funding their research staff training (FPI) grant.

References

1. T. Komljenovic, D. Huang, P. Pintus, M. A. Tran, M. L. Davenport, and J. E. Bowers, "Photonic Integrated Circuits Using Heterogeneous Integration on Silicon," Proc. IEEE **106**(12), 2246–2257 (2018).
2. M. He, M. Xu, Y. Ren, J. Jian, Z. Ruan, Y. Xu, S. Gao, S. Sun, X. Wen, L. Zhou, L. Liu, C. Guo, H. Chen, S. Yu, L. Liu, and X. Cai, "High-Performance Hybrid Silicon and Lithium Niobate Mach-Zehnder Modulators for 100 Gbit/s and Beyond," Nat. Photonics **13**, 359–364 (2019).
3. S. Abel, F. Eltes, J. E. Ortmann, A. Messner, P. Castera, T. Wagner, D. Urbonas, A. Rosa, A. M. Gutierrez, D. Tulli, P. Ma, B. Baeuerle, A. Josten, W. Heni, D. Caimi, L. Czornomaz, A. A. Demkov, J. Leuthold, P. Sanchis, and J. Fompeyrine, "Large Pockels effect in micro- and nanostructured barium titanate integrated on silicon," Nat. Mater. **18**(1), 42–47 (2019).
4. C. Haffner, D. Chelladurai, Y. Fedoryshyn, A. Josten, B. Baeuerle, W. Heni, T. Watanabe, T. Cui, B. Cheng, S. Saha, D. L. Elder, L. R. Dalton, A. Boltasseva, V. M. Shalaev, N. Kinsey, and J. Leuthold, "Low-loss plasmon-assisted electro-optic modulator," Nature **556**(7702), 483–486 (2018).
5. G. T. Reed, G. Mashanovich, F. Y. Gardes, and D. J. Thomson, "Silicon optical modulators," Nat. Photonics **4**(8), 518–526 (2010).
6. R. S. Jacobsen, K. N. Andersen, P. I. Borel, J. Fage-Pedersen, L. H. Frandsen, O. Hansen, M. Kristensen, A. V. Lavrinenko, G. Moulin, H. Ou, C. Peucheret, B. Zsigri, and A. Bjarklev, "Strained silicon as a new electro-optic material," Nature **441**(7090), 199–202 (2006).
7. M. Cazzanelli and J. Schilling, "Second order optical nonlinearity in silicon by symmetry breaking," Phys. Rev. Appl. **3**(1), 011104 (2016).
8. C. L. Manganelli, P. Pintus, and C. Bonati, "Modeling of strain-induced Pockels effect in Silicon," Opt. Express **23**(22), 28649–28666 (2015).
9. M. W. Puckett, J. S. T. Smalley, M. Abashin, A. Grieco, and Y. Fainman, "Tensor of the second-order nonlinear susceptibility in asymmetrically strained silicon waveguides: analysis and experimental validation," Opt. Lett. **39**(6), 1693–1696 (2014).

10. F. Bianco, K. Fedus, F. Enrichi, R. Pierobon, M. Cazzanelli, M. Ghulinyan, G. Pucker, and L. Pavesi, "Two-dimensional micro-Raman mapping of stress and strain distributions in strained silicon waveguides," Semicond. Sci. Technol. **27**(8), 085009 (2012).
11. B. Chmielak, C. Matheisen, C. Ripperda, J. Bolten, T. Wahlbrink, M. Waldow, and H. Kurz, "Investigation of local strain distribution and linear electro-optic effect in strained silicon waveguides," Opt. Express **21**(21), 25324–25332 (2013).
12. C. Schriever, F. Bianco, M. Cazzanelli, M. Ghulinyan, C. Eisenschmidt, J. Boor, A. Schmid, J. Heitmann, L. Pavesi, and J. Schilling, "Second-Order Optical Nonlinearity in Silicon Waveguides: Inhomogeneous Stress and Interfaces," Adv. Opt. Mater. **3**(1), 129–136 (2015).
13. B. Chmielak, M. Waldow, C. Matheisen, C. Ripperda, J. Bolten, T. Wahlbrink, M. Nagel, F. Merget, and H. Kurz, "Pockels effect based fully integrated, strained silicon electro-optic modulator," Opt. Express **19**(18), 17212–17219 (2011).
14. P. Damas, X. Le Roux, D. Le Bourdais, E. Cassan, D. Marris-Morini, N. Izard, T. Maroutian, P. Lecoeur, and L. Vivien, "Wavelength dependence of Pockels effect in strained silicon waveguides," Opt. Express **22**(18), 22095–22100 (2014).
15. S. Sharif Azadeh, F. Merget, M. P. Nezhad, and J. Witzens, "On the measurement of the Pockels effect in strained silicon," Opt. Lett. **40**(8), 1877–1880 (2015).
16. M. Borghi, M. Mancinelli, F. Merget, J. Witzens, M. Bernard, M. Ghulinyan, G. Pucker, and L. Pavesi, "High-frequency electro-optic measurement of strained silicon racetrack resonators," Opt. Lett. **40**(22), 5287–5290 (2015).
17. R. Sharma, M. W. Puckett, H. H. Lin, A. Isichenko, F. Vallini, and Y. Fainman, "Effect of dielectric claddings on the electro-optic behavior of silicon waveguides," Opt. Lett. **41**(6), 1185–1188 (2016).
18. M. Borghi, M. Mancinelli, M. Bernard, M. Ghulinyan, G. Pucker, and L. Pavesi, "Homodyne Detection of Free Carrier Induced Electro-Optic Modulation in Strained Silicon Resonators," J. Lit. Technol. **34**(24), 5657–5668 (2016).
19. I. Olivares, T. Angelova, and P. Sanchis, "On the influence of interface charging dynamics and stressing conditions in strained silicon devices," Sci. Rep. **7**(1), 7241 (2017).
20. C. Castellan, C. Vecchi, C. Ghulinyan, G. Pucker and L. Pavesi, "What is the role of trapped charges on the second harmonic generation in strained silicon waveguides?" in *International OSA Network of Students Yerevan 15* (Optical Society of America, 2018).
21. J. B. Khurgin, T. H. Stievater, M. W. Pruessner, and W. S. Rabinovich, "On the origin of the second-order nonlinearity in strained Si-SiN structures," J. Opt. Soc. Am. B **32**(12), 2494–2499 (2015).
22. P. Damas, D. Marris-Morini, E. Cassan, and L. Vivien, "Bond orbital description of the strain-induced second-order optical susceptibility in silicon," Phys. Rev. B **93**(16), 165208 (2016).
23. P. Damas, M. Berciano, G. Marcaud, C. Alonso, D. Marris-Morini, E. Cassan, and L. Vivien, "Comprehensive description of the electro-optic effects in strained silicon waveguides," J. Appl. Phys. **122**(15), 153105 (2017).
24. I. Avrutsky and R. Soref, "Phase-matched sum frequency generation in strained silicon waveguides using their second-order nonlinear optical susceptibility," Opt. Express **19**(22), 21707–21716 (2011).
25. M. Cazzanelli, F. Bianco, E. Borga, G. Pucker, M. Ghulinyan, E. Degoli, E. Luppi, V. Véniard, S. Ossicini, D. Modotto, S. Wabnitz, R. Pierobon, and L. Pavesi, "Second-harmonic generation in silicon waveguides strained by silicon nitride," Nat. Mater. **11**(2), 148–154 (2012).
26. C. Castellan, A. Trenti, C. Vecchi, A. Marchesini, M. Mancinelli, M. Ghulinyan, G. Pucker, and L. Pavesi, "On the origin of second harmonic generation in silicon waveguides with silicon nitride cladding," Sci. Rep. **9**(1), 1088 (2019).
27. C. Castellan, A. Trenti, M. Mancinelli, A. Marchesini, M. Ghulinyan, G. Pucker, and L. Pavesi, "From SHG to mid-infrared SPDC generation in strained silicon waveguides," Proc. SPIE **10358**, 1035804 (2017).
28. M. Berciano, G. Marcaud, P. Damas, X. Le Roux, P. Crozat, C. A. Ramos, D. Pérez, D. Benedikovic, D. Marris-Morini, E. Cassan, and L. Vivien, "Fast linear electro-optic effect in a centrosymmetric semiconductor," Commun. Phys. **1**(1), 64 (2018).
29. E. Timurdogan, C. V. Poulton, M. J. Byrd, and M. R. Watts, "Electric field-induced second-order nonlinear optical effects in silicon waveguides," Nat. Photonics **11**(3), 200–206 (2017).
30. J. J. Wortman and R. A. Evans, "Young's Modulus, Shear Modulus, and Poisson's Ratio in Silicon and Germanium," J. Appl. Phys. **36**(1), 153–156 (1965).
31. M. A. Hopcroft, W. D. Nix, and T. W. Kenny, "What is the Young's Modulus of Silicon?" J. Microelectromech. Syst. **19**(2), 229–238 (2010).
32. A. Yariv and P. Yeh, *Optical Waves in Crystals* (Wiley, 1984).